Electron transport in a Pt-CO-Pt nanocontact: First-principles calculations

M. Strange, K. S. Thygesen, and K. W. Jacobsen

Center for Atomic-scale Materials Physics, Department of Physics

NanoDTU, Technical University of Denmark, DK-2800 Kgs. Lyngby, Denmark

(Dated: November 12, 2018)

We have performed first-principles calculations for the mechanic and electric properties of pure Pt nano-contacts and a Pt contact with a single CO molecule adsorbed. For the pure Pt contacts we see a clear difference between point contacts and short chains in good agreement with experiments. We identify a tilted bridge configuration for the Pt-CO-Pt contact, which is stable and has a conductance close to $0.5G_0$ ($G_0 = 2e^2/h$), and we propose that this structure is responsible for an observed peak at $0.5G_0$ in the conductance histogram for Pt exposed to a CO gas. We explain the main features of the transmission function for the Pt-CO-Pt contact, and show that the conductance is largely determined by the local d-band at the Pt apex atoms.

PACS numbers: 73.63.Rt, 73.20.Hb, 73.40.Gk

I. INTRODUCTION

Advances in the experimental techniques for manipulating and contacting individual atoms and molecules, and the vision of using simple organic molecules as the basic building blocks in electronic devices, have recently intensified the interest for electron transport in nanoscale contacts. ^{1,2,3,4} On the theoretical side a number of first principles methods to describe the electrical properties of realistic atomic-sized junctions have been developed. ^{5,6,7,8,9} Many of these methods combine a single-particle description of the electronic structure extracted from density functional theory (DFT), ¹⁰ with a non-equilibrium Green's function formalism¹¹ to calculate the current. The various schemes mainly differ in the choices of basis sets and the way in which the coupling between the molecule and macroscopic leads is taken into account.

Regardless of the details of the implementation, the LDA/GGA DFT based transport schemes show the same general trend: the calculated conductance for molecular contacts in the low-conducting regime, i.e. contacts with a conductance much lower than the conductance unit $G_0 = 2e^2/h$, is 2-3 orders of magnitude higher than corresponding experimental values. 12,13,14,15,16 A number of reasons for this discrepancy have been proposed, including correlation effects not captured by the mean-field approach^{17,18} and differences between the atomic structures used in the calculations and those realized under experimental conditions. 13,15 On the other hand, a most satisfactory agreement between DFT based calculations and experiments is found for the conductance of homogeneous metallic point contacts and monatomic wires. For these systems, both the size of the conductance, the number of conductance channels, and the so-called conductance oscillations are well reproduced by calculations 5,7,19,20,21,22,23,24,25,26 The same good agreement between theory and experiment has been found for a heterogeneous molecular junction consisting of a single hydrogen molecule captured between Pt electrodes. 27,28,29 Common to all these systems, for which DFT provides a description of the transport in agreement with experiment, is that the coupling to the metallic leads is strong and the conductance is high, i.e. on the order of $1G_0$.

There remains much to be learned about the reasons for these apparent trends in DFT based transport calculations and it is therefore desirable to extent the knowledge of systems, for which transport properties can be treated within the framework of DFT.

In this paper we present DFT calculations for pure Pt contacts and a Pt-CO-Pt system, which according to experiments have a conductance on the order of $1G_0$ and thus belongs to the group of systems for which previous DFT transport calculations have been successful. We have calculated the total energy and conductances of pure Pt contacts and chains as well as for Pt contacts with a single CO molecule adsorbed. Our main result is the identification of a certain "tilted bridge" configuration for the Pt-CO-Pt contact which is energetically stable and has a conductance close to $0.5G_0$ in agreement with recent experimental results.³⁰ We find that the transport properties of the Pt-CO-Pt junction to a large extend are determined by the properties of the bare Pt electrodes. For this reason we put some emphasis on verifying the ability of our method to reproduce key characteristics of the transport properties of pure Pt contacts and chains. Also here we find good agreement with experiments.

Mechanically controlled break junction experiments performed at cryogenic temperature on pure Pt samples show, that as a Pt contact is pulled apart a structure with a characteristic conductance of around $1.5G_0$ is formed in the last stages before the contact breaks. This is inferred from conductance histograms 30,31,32 which show a pronounced peak at this value. In addition to the peak at $1.5G_0$, many histograms on Pt contain a smaller and broader peak at around $2.1G_0$. The two peaks are believed to correspond to chains and atomic point contacts, respectively. The fact that the peak at $1.5G_0$ is higher than the peak at $2.1G_0$ is explained by the suppression of point contacts by the formation of chains. Experimental evidence for this hypothesis comes from conductance histograms recorded as the broken contacts are brought back into contact – the so-called return histograms. Such histograms contain no contributions from chains, and show a single peak at $2.1G_0$.³¹ Our calculations predict that Pt point contacts have a conductance of $(2.0-2.3)G_0$, whereas short Pt chains have a conductance of $(1.3-2.0)G_0$ in good agreement with the experimental findings.

When the Pt contact is exposed to a CO gas, the peaks characteristic for pure Pt disappears from the conductance histogram and are instead replaced by two peaks at $\sim 0.5G_0$ and $\sim 1.1G_0$. The physical origins of these peaks have not been identified experimentally. Recent measurements on magnetic as well as non-magnetic metal point contacts³³, showed a fractional conductance of $0.5G_0$, and this was interpreted as the lifting of a spin-degenerate conductance channel. However, none of these results could be reproduced in experiments by C. Untiedt and co-workers. 30 Instead, they suggested that the reported fractional conductances could result from CO contamination. Regardless of whether CO is the source of the reported fractional conductances, the question of the physical mechanism of the peak at $0.5G_0$ in the Pt-CO-Pt histogram still remains: is it a spin effect or does it have some other origin?

On the basis of our calculations we propose that the $0.5G_0$ peak in the Pt-CO-Pt histogram is due to a configuration where a single CO molecule provides a "tilted bridge" between two Pt apex atoms. We find that this structure has a conductance just below $0.5G_0$ for a wide range of electrode displacements leading to a plateau in the conductance trace. By carrying out a Wannier function analysis we identify the current carrying states of the molecule as the $2\pi^*$ CO orbitals. However, the main features of the transmission function are not determined by these orbitals but rather by the Pt d-band at the apex atoms. The fact that the Pt-C bond is much stronger than the Pt-O bond allows us to simplify a resonant level model for asymmetric coupling, and obtain a simple description of the transmission function in terms of a single d-like Pt orbital, the energy level of the $2\pi^*$ CO orbital, and a coupling strength. All the parameters of the model are extracted from the first principles calculations.

The paper is organized as follows. In Sec. II we outline our Wannier function based transport scheme. In Sec. III we present the results for simulated conductance traces of pure Pt point contacts and short Pt chains. In Sec. IV the Pt-CO-Pt system is investigated by simulating a conductance trace and identifying the origin of the main features of the transmission function. Finally, Sec. V contains a summary.

II. METHOD

In this section we briefly review the computational methods used in the present study. All total energy calculations are performed using a plane wave implementation of density functional theory.³⁴ The nuclei and core electrons are described by ultra-soft pseudopotentials³⁵,

and exchange and correlation is treated at the GGA level using the PW91 energy-functional. The Kohn-Sham (KS) eigenstates are expanded in plane waves with a kinetic energy less than 25Ry. Optimizations of all the considered structures have been performed, until the total residual force is below $0.05 {\rm eV/\AA}$.

The electrical conductance is evaluated within the Landauer-Bütikker formalism. Thus the system is divided into three regions: a left lead (L), a right lead (R), and a central region (C). The leads are assumed to be perfect conductors such that all scattering takes place in C. The linear response conductance due to scattering upon C is given by $G = G_0T(\varepsilon_F)$, where $T(\varepsilon_F)$ is the elastic transmission function evaluated at the Fermi energy. Here we evaluate $T(\varepsilon)$ from the self-consistent KS Hamiltonian, which we represent in terms of a basis consisting of maximally localized, partly occupied Wannier functions (WFs). The WFs are constructed according to a recently developed method^{37,38,39} in such a way, that the KS eigenstates are exactly reproducible in terms of the WFs within some specified energy window. The energy window is typically selected to include all eigenstates up to around 4eV above the Fermi level, and thus the plane wave accuracy of the original DFT calculation is retained in the subsequent transport calculation. The use of a localized basis set allows us to calculate $T(\varepsilon)$ using the general non-equilibrium Green's function formalism.⁴⁰ This formalism is formulated in terms of orthogonal basis functions, but was recently generalized to the case of non-orthogonal basis functions.⁴¹

Furthermore, the formalism is generally valid for a finite bias voltage, however, in this study we shall focus on the linear response conductance.

III. PT POINT CONTACTS AND CHAINS

In this section we investigate the electrical properties of pure Pt contacts and short Pt chains between bulk Pt electrodes. This study serves a dual purpose. First, it provides a theoretical justification for assigning the two peaks at $1.5G_0$ and $2.1G_0$ in the conductance histograms for Pt to chains and point contacts, respectively. Secondly, it allows us to test the ability of the calculational scheme against well established experimental results and other computer simulations before applying it in the study of the Pt-CO-Pt contact.

The Pt contacts are modeled using supercells by two 4-atom pyramids oriented towards each other and attached to Pt(111) surfaces containing 3x3 atoms in the surface plane. Two different structures are considered: (i) A point contact, where the apex atoms of the pyramids are in direct contact. (ii) A 1-atom chain, where a single Pt atom is inserted between the apex atoms of the pyramids, see Fig. 1. In order to ensure that the effective KS potential has converged to its bulk values at the end planes of the supercell we include 3-4 atomic layers on either side of the pyramids.

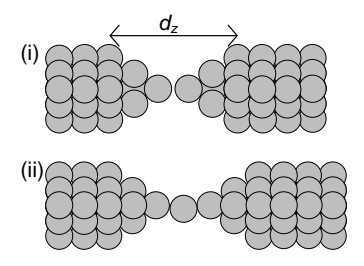


FIG. 1: Supercells used to model the two considered structures: (i) A point-contact, and (ii) a 1-atom chain. The electrode displacement d_z is defined as the distance between the (111) surfaces.

For the total energy calculations, the Brillouin zone (BZ) is sampled by a $4\times4\times1$ Monkhort-Pack grid. ⁴² The transmission function is sampled over a 4×4 **k**-point grid in the two dimensional BZ of the surface plane. This sampling is crucial in order to avoid unphysical features in the transmission functions due to Van Hove singularities associated with the quasi-one dimensional leads. ⁴³

A. Pt point contact

By increasing the electrode displacement d_z , defined as the distance between the fixed (111) surfaces (see Fig. 1), and relaxing the pyramids at each step before calculating the conductance, we simulate the process of creating a conductance trace. The result for the point contact is shown in Fig. 2, where the triangles denote conductances and the circles denote the total energies measured relative to the first configuration ($d_z = 10.9 \text{Å}$).

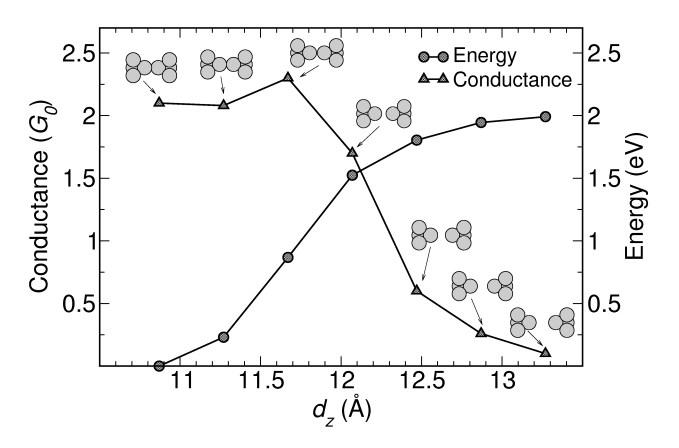


FIG. 2: Conductance (triangles) and total energy (circles) for the Pt point contact as a function of electrode displacement d_z .

For the first three configurations, the conductance stays just above $2G_0$. The reason for the relatively weak changes in the conductance in this region, is that the elongation occurs quite uniformly over the pyramids, such that the distance between the apex atoms changes only slightly. At configuration four $(d_z = 12.07\text{Å})$ the

bond between the two apex atoms is broken, which can be seen directly from the insets. The breaking of the central bond marks the onset of a structural relaxation, which affects both the conductance and force significantly. Beyond this point the contact enters the tunneling regime and the conductance decreases exponentially.

The simulated conductance trace is in good agreement with the experimental return histograms for Pt^{31} which show a peak around $2.1G_0$. Moreover, both the plateau around $2G_0$ as well as the rate of the exponential decay in the tunneling regime compare well with the calculations reported in Ref. 26.

B. Short Pt chain

We have simulated the breaking of a one-atom Pt chain following the same procedure as for the point contacts described in the preceding subsection. The results are shown in Fig. 3. The calculated conductance trace has

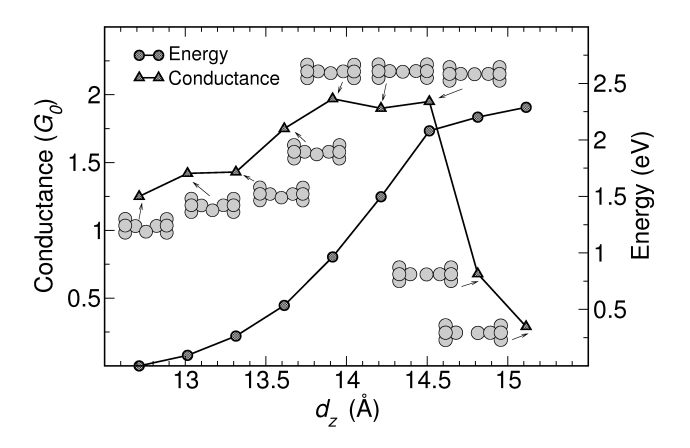


FIG. 3: Conductance (triangles) and total energy (circles) as a function of electrode displacement, d_z .

a plateau at around $1.4G_0$ for small d_z where the chain zigzags. As the contact is stretched further the conductance rises to a conductance just below $2G_0$, before the contact breaks at $d_z = 14.5$ Å. At this point the structure relaxes towards the surfaces, and the conductance starts to decay exponentially as the tunneling regime is entered. The correlation between structural relaxations and sharp changes in the conductance is a characteristic feature of the contact formation process. The effect has been observed experimentally for gold chains by measuring the conductances and forces simultaneously.^{44,45} Furthermore, we notice that the increase in the conductance just before the contact breaks, seen in both Fig. 2 and Fig. 3, is also observed experimentally, and is in fact characteristic of conductance traces for Pt and Al contacts.³² In the case of Pt this behavior could be related to the linearizion of the chains which activates more conductance channels.²⁶ A similar explanation has been given in the case of Al contacts. 23,24

Finally, we stress that in order to obtain plateaus in a

simulated conductance trace and thus predict the occurrence of peaks in a conductance histogram, it is necessary to allow the central atoms of the contact to relax in the elongation process.

IV. PT-CO-PT CONTACT

As discussed in Sec. I, the controlled exposure of the Pt contact to a CO gas changes the conductance histogram completely: the peaks at $1.5G_0$ and $2.1G_0$ characteristic of pure Pt are replaced by peaks at $0.5G_0$ and at $1.1G_0$. In order to understand the physical origin of the new peaks, we have carried out total energy and conductance calculations using the same setup as for the pure Pt contacts discussed in the preceding section.

The results are summarized in Fig. 4, where we show the conductance (triangles) and total energy (circles) as a function of the electrode displacement d_z . For the ini-

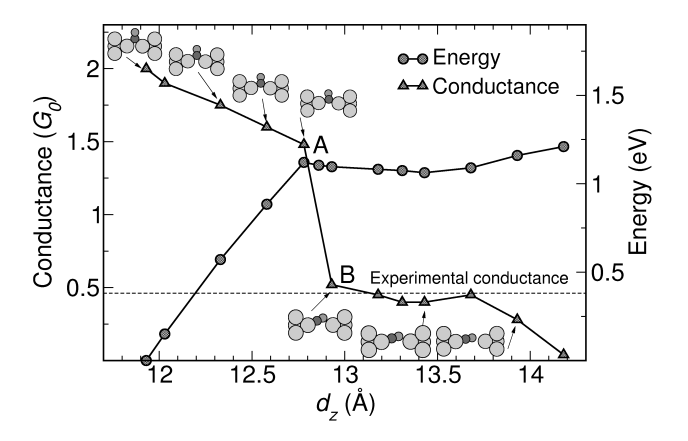


FIG. 4: Conductance (triangles) and total energy (circles) as a function of electrode displacement d_z . The conductance trace is divided into an upper and a lower part, corresponding to the CO in the upright bridge- and tilted bridge configuration, respectively. A and B labels the configurations just before and just after CO has tilted, respectively.

tial contact geometry and small d_z , CO is most stable at the central Pt-Pt bridge of the contact, bonding symmetrically with C to the two Pt atoms in an upright bridge configuration. It is seen that the conductance decreases linearly from $2.1G_0$ to $1.5G_0$ as the upright bridge configuration is being stretched. At $d_z=12.8\text{\AA}$ one of the C-Pt bonds breaks, and the contact relaxes to a tilted bridge configuration. This qualitative change in the atomic structure is clearly seen in the conductance which jumps abruptly from $\sim 1.5G_0$ to a plateau at $\sim 0.5G_0$ which then extends over almost 1\AA .

In order for the upright and tilted bridge configurations to be observed with a reasonable probability in the experiment, the binding energy of CO in these positions should be larger than that of CO adsorbed on the nearby sites, i.e. on the (111)-surface sites. This is indeed the case, as the binding energy for the upright and tilted bridge is around -2.6eV, while that of CO on Pt (111) varies between -0.3eV and -1.8eV, depending on the coverage. 46,47

Whether the conductance plateau at $0.5G_0$ in Fig. 4 will contribute to a peak in a conductance histogram, depends crucially on the stiffness k_s of the Pt electrodes.⁴⁸ Each Pt electrode can be viewed as a spring connected to the CO contact, and in our setup only the relaxation of the atoms near to the CO molecule have been taken into account. These local relaxations are very important and responsible for the abrupt drop in the conductance curve. However, to obtain a more realistic conductance trace, the finite spring constant of the remaining electrodes should be taken into account, and this will deform the x-axis in Fig. 4. We make the assumption that at some points far away from the contact, the position of the electrodes are controlled and denote the separation between these points by L. The relation between L and the distance between the Pt surfaces, d_z , can be obtained by solving the equation

$$\frac{1}{2}k_s(L-d_z) = \frac{\partial E(d_z)}{\partial d_z},\tag{1}$$

which expresses the force balance between the springs (left hand side) and the contact region (right hand side). The factor 1/2 is due to the fact that each springs are acting on both sides of the contact, with a stiffness of k_s .

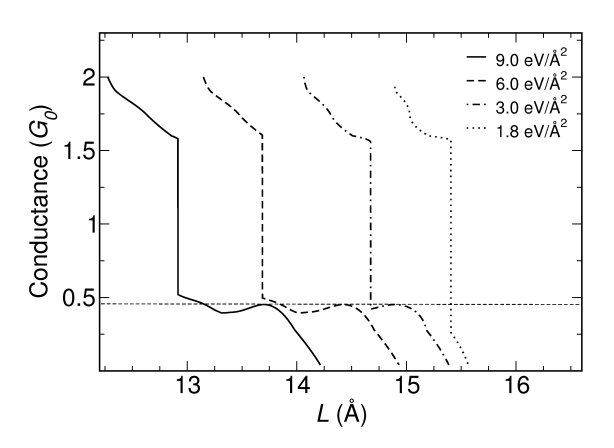


FIG. 5: Conductance traces for different values of the electrode stiffness, k_s . The size of k_s determines the length of the conductance plateau at $0.5G_0$: a stiff electrode (large k_s) results in a long plateau, while a soft electrode (small k_s) results in a short or no plateau.

In Fig. 5, we show the corrected conductance traces for k_s between 1.8 eV/Å² and 9.0 eV/Å². For k_s below ~ 2 eV/Å², the $0.5G_0$ conductance plateau is completely absent and the tilted bridge configuration would not contribute to the conductance histogram. However, when $k_s > 3$ eV/Å² the $0.5G_0$ plateau becomes clearly visible, and would lead to a peak at $0.5G_0$ in the conductance histogram. Experimental estimates for k_s do not exist for Pt electrodes, however, in the case of gold

values in the range 0.2eV/Å^2 to 4eV/Å^2 have recently been reported, on the basis of non-exponential distance dependence of the tunneling current.⁴⁹

We therefore propose, that the observed peak in the conductance histogram for CO in Pt nanocontacts is due to the tilted bridge configuration. All our calculations are averaged over spin, and the special conductance of $0.5G_0$ is therefore not related to spin. This is further illustrated below, where we study the transport mechanism in more detail.

Finally, we mention that the peak around $1.1G_0$ in the experimental histograms, cannot be explained by our calculations for a single CO molecule in the Pt contact. We have also calculated the conductance of the CO bridge in the one atom chain in search of a structure that can explain the peak at $1.1G_0$, however, we found conductances quite similar to those obtained for CO in the Pt point contact.

A. Conduction mechanism

In this section we address the question of the physical origin of the fractional conductance of $0.5G_0$ found for the tilted bridge configuration. Fig. 6 shows a typical transmission function for the upright bridge configuration (dashed line) and tilted bridge configuration (full line) immediately before and after the bridge tilts – configurations A and B in Fig. 4. The dotted line denotes the transmission function obtained for configuration B with a localized atomic-like basis set taken from the DFT code Siesta.⁵⁰ The transmission function has been averaged over the same k-points and calculated using the same electron transport code as the WFs transmission functions. The basis set used is the Siesta "default" double zeta with polarizations functions (DZP) in combination with Troullier-Martins pseudopotentials.⁵¹ Exchange and correlation are described by the PBE functional, ⁵² which is close to PW91 used in the WFs calculations. The transmission functions obtained using the two different DFT-codes are seen to be in good agreement, especially in the important region near the Fermi-level. We have observed similar good agreements for the other Pt-CO-Pt structures considered in this work. This indicates that our results are independent of the basis set and other technical details related to the calculation of the selfconsistent KS-Hamiltonian.

In both cases (A and B) there is a pronounced resonance at the Fermi level, which clearly is responsible for the conductance of $1.5G_0$ and $0.5G_0$, respectively. In fact this resonance is present for all the configurations investigated in this study, and it therefore represents a very general and robust feature of the transport through a Pt-CO-Pt contact. As the following analysis will show, the resonance is not due to the CO molecule alone, but rather is a (local) band structure effect related to the d-orbitals at the Pt apex atoms.

To address the origin of the resonance, we perform an

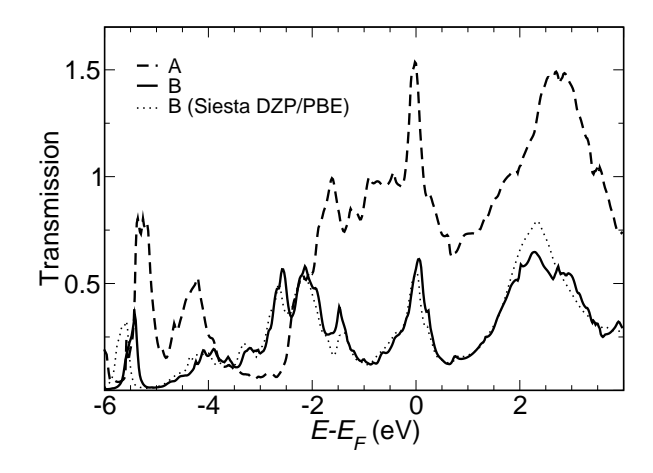


FIG. 6: Typical transmission function for the upright bridge (configuration A in Fig. 4) and the tilted bridge (configuration B). The dotted line is the transmission function obtained using Siesta-DZP/PBE. Both transmission functions (A and B) have a resonance at the Fermi level which can be related to the density of states of the so-called group orbitals.

analysis of the local electronic structure in the contact region by diagonalizing the Hamiltonian within the subspace spanned by the WFs located at the CO molecule. The orbitals and eigenvalues obtained in this way represent renormalized energy levels of the CO molecule including the effect of the coupling to the Pt leads. For all the considered contact geometries we find seven WFs located at the CO molecule, leading to seven renormalized molecular energy levels. For simplicity we focus on the tilted CO bridge in the following (configuration B), however, the conclusions are also valid for the upright bridge configuration. Since CO has 10 valence electrons, the seven renormalized CO orbitals represent the five occupied and the two lowest unoccupied molecular orbitals. The latter are the $2\pi^*$ orbitals which are known to be important for the chemisorption properties of $CO.^{47,53,54}$ By repeating the conductance calculations with the renormalized $2\pi^*$ orbitals removed from the basis set, we find that the resonance at the Fermi level is completely gone and the conductance is reduced to $\sim 0.05G_0$. This allows us to focus exclusively on the $2\pi^*$ CO orbitals when analyzing the transport properties of the Pt-CO-Pt contacts. In the following we will refer to the $2\pi^*$ states as $|a\rangle$ and $|b\rangle$. The on-site energies of these renormalized orbitals are $\varepsilon_a = 1.5 \text{ eV}$ and $\varepsilon_b = 1.6 \text{ eV}$, respectively. The splitting of the levels is induced by the different couplings to the electrodes.

Each of the molecular orbitals (MO) $|a\rangle$ and $|b\rangle$ give rise to one transmission channel through the CO molecule. If we neglect tunneling due to direct coupling between the Pt apex atoms, and neglect interference between the two transport channels, we can analyze the problem by considering the transport through each MO separately. We do this using the well known single-level model for resonant transport. A particularly simple form of the single level model, is obtained by intro-

ducing the so-called group orbitals.⁵⁵ The group-orbital for MO $|a\rangle$ (or $|b\rangle$) of lead α ($\alpha=L,R$) is defined as $|g_{\alpha}^{a}\rangle=\frac{1}{V_{\alpha,a}}P_{\alpha}H|a\rangle$, where H is the Hamiltonian, P_{α} is the orthogonal projection onto lead α , and $1/V_{\alpha,a}$ a normalization constant. The name "group orbital" refers to the fact that $|g_{\alpha}^{a}\rangle$ consists of the group of states in the lead to which $|a\rangle$ is most strongly coupled. In fact, the coupling between $|a\rangle$ and any state in lead α orthogonal to $|g_{\alpha}^{a}\rangle$ is zero, while the coupling to the group orbital is given by $V_{\alpha,a}=\langle a|H|g_{\alpha}\rangle$. In the limit of strong asymmetric coupling, when $V_{R,a}^{2}<< V_{L,a}^{2}$, the transmission function takes the form

$$T(\varepsilon) = 4\pi^2 V_{R,a}^2 \rho_{R,a}^0(\varepsilon) \rho_a(\varepsilon), \tag{2}$$

where $\rho_a(\varepsilon)$ is the projected density of states (PDOS) of the MO $|a\rangle$ and $\rho_{R,a}^0(\varepsilon)$ is the PDOS of the group orbital of the right lead in the absence of coupling to $|a\rangle$, i.e. calculated with $V_{R,a}=0$. The limit of strong asymmetric coupling is relevant for the tilted bridge configuration where $V_R^2/V_L^2\approx 0.1$ for both MOs $|a\rangle$ and $|b\rangle$. The large asymmetry in the coupling strengths indicates that the Pt-C bond is much stronger than the Pt-O bond. To illustrate the situation, the inset of Fig. 7 shows an isosurface plot of $|a\rangle$ (transparent) together with its left and right group orbitals (solid). The latter consists mainly of d-like orbitals centered on the apex Pt atoms. The coupling strengths $V_{L,a}$ and $V_{R,a}$ are indicated.

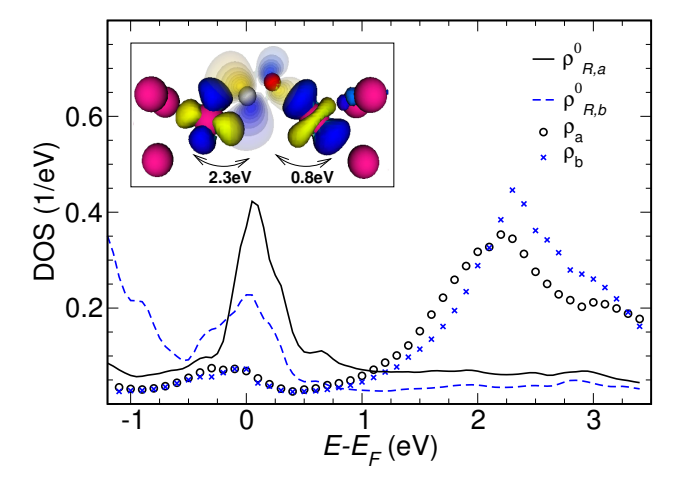


FIG. 7: (Color online) The PDOS of the $2\pi^*$ states $|a\rangle$ and $|b\rangle$ together with the PDOS of the group orbital in the weakly coupled right lead. The inset shows an iso-surface plot of the MO $|a\rangle$ (transparent) and its corresponding left and right group orbitals (solid). The PDOS for the MOs (circles and stars) is quite flat around the Fermi level, while the the PDOS of two group orbitals (full and dashed lines) both have a peak at the Fermi level. It is this peak that gives rise to the resonance in the transmission function.

According to Eq. (2) the energy dependence of the transmission function is determined by the product of the PDOS of the MO and the PDOS of the group orbital in the weakly coupled lead. In Fig. 7 we show the calculated PDOS for the MOs $|a\rangle$ and $|b\rangle$ together with

the PDOS of the corresponding group orbitals $|g_R^a\rangle$ and $|g_R^b\rangle$. It is now clear that the transmission resonance at the Fermi level results from a corresponding peak in the PDOS of the group orbitals of the right lead, or, equivalently, from a peak in the PDOS of the d-states at the Pt apex atoms. The bare energies of the MOs at $\varepsilon_a=1.5 \mathrm{eV}$ and $\varepsilon_b=1.6 \mathrm{eV}$, respectively, are shifted upwards by the coupling to the Pt d-band, and can be seen as broad peaks in the PDOS at $\sim 2.2 \mathrm{eV}$. These peaks are also clearly visible in the transmission function in Fig. 6.

The transmission resonance at E_F is thus caused by the properties of the isolated Pt lead, while the role of the $2\pi^*$ CO orbitals is to provide a flat background at the Fermi level and a peaked structure at $\sim 2.2 \text{eV}$. Since the group orbitals for different configurations are very similar (always d-like) the determining factors in the transmission functions stay almost constant, and this explains the robustness of the main features in the transmission function.

It is well known, that the calculated HOMO-LUMO gap of CO is somewhat sensitive to the applied exchange-correlation functional. However, since the transport properties of the investigated Pt-CO-Pt bridge involves only the tails of the PDOS of the CO orbitals and is dominated by the PDOS of the Pt leads, the exact positions of the CO energy levels are not expected to be crucial. An accurate description of Pt is, however, important and as discussed in Sec. III our results for Pt are in good agreement with experiments.

V. SUMMARY

We have performed calculations within the framework of density functional theory for the mechanical and electrical properties of pure Pt nano-contacts and Pt contacts with a single CO molecule.

For the pure Pt contacts, we obtain conductances traces which are in good agreement with experiments as well as other recent theoretical calculations. Our results show that Pt point contacts have a conductance in the range $(2.0-2.3)G_0$ while that of short Pt chains is $(1.3-2.0)G_0$. This provides a theoretical justification for assigning the peaks at $\sim 2.1G_0$ and $\sim 1.5G_0$ in the conductance histogram for Pt to point contacts and chains, respectively.

For the Pt-CO-Pt contact we identify an energetically stable configuration with the CO molecule providing a tilted bridge between two Pt apex atoms. Based on realistic DFT simulations of the creation of a conductance trace with the elastic response of the electrodes included through effective spring constants, we propose that the tilted CO bridge is responsible for the peak at $0.5G_0$ observed recently in the conductance histogram for Pt-CO-Pt. We characterize and explain the main features of the transmission function for the Pt-CO-Pt contact in terms of the properties of the isolated CO molecule and the free Pt leads. The analysis shows that the conductance

to a large extent is determined by the local d-band at the Pt apex atoms and to a smaller extent by the $2\pi^*$ CO orbitals.

kic for illuminating discussions on the interpretation of their break-junction experiments. We acknowledge support from the Danish Center for Scientific Computing through Grant No. HDW-1101-05.

VI. ACKNOWLEDGMENTS

We would like to thank J. van Ruitenbeek and D. Dju-

- ¹ H. Ohnishi, Y. Kondo, and K. Takayanagi Nature (London) **344**, 524 (1998).
- ² C. Joachim, J. K. Gimzewski and A. Aviram Nature (London) 408, 541 (2000).
- ³ A. Aviram and M. A. Ratner, Chem. Phys. Lett. 29, 277 (1974).
- ⁴ D. M. Eigler and E. K. Schweizer Nature **344**, 56 (1991).
- ⁵ Y. Fujimoto and K. Hirose Phys. Rev. B **67**, 195315 (2003).
- ⁶ A. R. Rocha, V. M. García-Suárez, S. W. Baily, C. J. Lambert, J. Ferrer and S. Sanvito Nature Materials 4, 335 (2005).
- M. Brandbyge, J. L. Mozos, P. Ordejón, J. Taylor, and K. Stokbro Phys. Rev. B 65,165401 (2002).
- ⁸ Y. Xue, S. Datta, and M. A. Ratner Chem. Phys **281**, 151 (2002).
- ⁹ A. Calzolari, N. Marzari, I. Souza, M. B. Nardelli Phys. Rev. B **69**, 35108 (2004).
- ¹⁰ W. Kohn and L. J. Sham Phys. Rev. **140** (1965).
- ¹¹ L. V. Keldysh Soviet Physics JETP-USSR **20**, 1018 (1965).
- ¹² J. Heurich, J. C. Cuevas, W. Wenzel, and G. Schön Phys. Rev. Lett. 88, 256803 (2002).
- ¹³ M. Di Ventra, S. T. Pantelides, and N. D. Lang Phys. Rev. Lett. **84**, 979 (2000).
- ¹⁴ P. A. Derosa and J. M. Seinario J. Phys. Chem. B **105**, 471 (2001).
- ¹⁵ K. Stokbro, J. Taylor, M. Brandbyge, J.-L. Mozos, and P. Ordejn Comp. Matt. Science 27, 151 (2003).
- Y. Xue and M. A. Ratner Int. J. Quantum Chem. 102, 911 (2005).
- ¹⁷ P. Delaney and J. C. Greer Phys. Rev. Lett. **93**, 036805 (2004).
- ¹⁸ A. Ferretti, A. Calzolari, R. Di Felice, F. Manghi, M.J. Caldas, M. B. Nardelli, and E. Molinari Phys. Rev. Lett. **94**, 116802 (2005).
- A. Nakamura, M. Brandbyge, L. B. Hansen, and K. W. Jacobsen Phys. Rev. Lett. 82, 1538 (1999).
- J. J. Palacios, A. J. Pérez-Jiménez, E. Louis, E. SanFabián, and J. A. Vergés Phys. Rev. B 66, 35322 (2002).
- Y. J. Lee, M. Brandbyge, M. J. Puska, J. Taylor, K. Stokbro, and R. M. Nieminen Phys. Rev. B 69, 125409 (2004).
- ²² T. Ono and K. Hirose Phys. Rev. B **70**, 33403 (2004).
- ²³ P. Jelínek, R. Pérez, J. Ortega, and F. Flores Phys. Rev. B **68**, 085403 (2003).
- ²⁴ N. Kobayashi, M. Brandbyge, and M. Tsukada Phys. Rev. B **62**, 8430 (2000)
- ²⁵ Elke Scheer, Nicolás Agraït, Juan Carlos Cuevas, Alfredo Levy Yeyati, Bas Lodoph, Alvaro Martín-Rodero, Gabino Rubio Bollinger, Jan M. van Ruitenbeek and Christián Urbina Nature 394,154 (1998)
- ²⁶ V. M. García Suárez, A. R. Rocha, S. W. Bailey, C. J. Lam-

- bert, S. Sanvito, and J. Ferrer cond-mat/0505487
- ²⁷ R. H. M Smit, Y. Noat, C. Untiedt, N. D. Lang, M. C. van Hemert, and J. M. van Ruitenbeek Nature (London) 419, 906 (2002)
- ²⁸ K. S. Thygesen and K. W. Jacobsen, Phys. Rev. Lett. **94**, 036807 (2005).
- ²⁹ V. M García-Suárez, A. R. Rocha, S. W. Bailey, C. J. Lambert, S. Sanvito, and J. Ferrer Phys. Rev. B **72**, 045437 (2005)
- ³⁰ C. Untiedt, D. M. Dekker, D. Djukic, and J. M. van Ruitenbeek Phys. Rev. B **69**, 0.81401 (2004).
- ³¹ S. K. Nielsen, Y. Noat, M. Brandbyge, R. H. M. Smit, K. Hansen, L. Y. Chen, A. I. Yanson, F. Besenbacher, and J. M. van Ruitenbeek Phys. Rev. B 67, 245411 (2003).
- ³² J. M. Krans, C. J. Muller, I. K. Yanson, T. C. M. Govaert, R. Hesper, and J. M. van Ruitenbeek Phys. Rev. B 48, R14721 (1993).
- ³³ V. Rodrigues, J. Bettini, P. C. Silva, and D. Ugarte Phys. Rev. Lett. **91**, 096801 (2003).
- ³⁴ B. Hammer, L.B. Hansen, and J.K. Nørskov, Phys. Rev. B **59**, 7413 (1999); S.R. Bahn and K.W. Jacobsen, Comp. Sci. Eng. **4**, 56 (2002); The Dacapo code can be downloaded at http://www.fysik.dtu.dk/campos.
- ³⁵ D. Vanderbilt, Phys. Rev. B **41**, R7892 (1990).
- ³⁶ J. P. Perdew *et al.*, Phys. Rev. B **46**, 6671 (1992).
- 37 K. S. Thygesen and K. W. Jacobsen, arXiv:cond-mat/0501238, (Submitted to Chem. Phys.)
- ³⁸ K. S. Thygesen, L. B. Hansen and K. W. Jacobsen, Phys. Rev. Lett. **94**, 026405 (2005).
- ³⁹ K. S. Thygesen, L. B. Hansen and K. W. Jacobsen, Phys. Rev. B **72**, 125119 (2005)
- ⁴⁰ Y. Meir and N. S. Wingreen, Phys. Rev. Lett. **68**, 2512 (1992).
- ⁴¹ K. S. Thygesen, arXiv:cond-mat/0509317
- ⁴² H. J. Monkhorst and J. D. Pack Phys. Rev. B **13**, 5188 (1976).
- ⁴³ K. S. Thygesen and K. W. Jacobsen cond-mat/0411589
- ⁴⁴ G. Rubio-Bollinger, S. R. Bahn, N. Agrait, K. W. Jacobsen, S. Vieira Phys. Rev. Lett. 87, 026101 (2001)
- ⁴⁵ G. Rubio, N. Agrait, and S. Vieira Phys. Rev. Lett. **76**, 2302 (1996)
- ⁴⁶ J. A. Steckel, A. Eichler, and J. Hafner Phys. Rev. B 68, 85416 (2003)
- ⁴⁷ K. Doll Surface Science **573**, 464 (2004).
- ⁴⁸ M. Brandbyge, M. R. Sørensen, and K. W. Jacobsen Phys. Rev. B **56**, 14956 (1997)
- ⁴⁹ G. Rubio-Bollinger, P. Joyez, and N. Agrait Phys. Rev. Lett. **93**, 116803 (2004)
- J. M. Soler, E. Artacho, J. D. Gale, A. García, J. Junquera, P. Ordejón and D. Sanchez-Portal J. Phys. Cond. Matter

- **14**, 2745-2779 (2002).
- ⁵¹ N. Troullier and J. L. Martins Solid State Commun. **74**,
- ⁵² J. P. Perdew, K. Burke, and M. Ernzerhof Phys. Rev. Lett. **77**, 3865 (1996)
- 53 G. Blyholder J. Phys. Chem. **68**, 2772 (1964).
 54 B. Hammer, Y. Morikawa and J. K. Nørskov Phys. Rev. Lett. **76**, 2141 (1996).
- 55 M. J. Kelly in Solid State Physics, Volume 35, H. Ehrenreich, F. Seitz, and D. Turnbull (Eds.), (Academic Press,
- New York, 1980), page 333

 56 A. I. Yanson, G. Rubio Bollinger, H. E. van der Brom, N. Agrait, and J. M. Ruitenbeek Nature (London) 395, 783 (1998).